THE JOURNAL OF BIOLOGICAL CHEMISTRY VOL. 291, NO. 44, pp. 23136–23148, October 28, 2016

The C-terminal Helix of *Pseudomonas aeruginosa* Elongation Factor Ts Tunes EF-Tu Dynamics to Modulate Nucleotide Exchange*

Received for publication, May 26, 2016, and in revised form, September 12, 2016 Published, JBC Papers in Press, September 13, 2016, DOI 10.1074/jbc.M116.740381

Evelina Ines De Laurentiis, Evan Mercier, and Hans-Joachim Wieden[1]

From the Department of Chemistry and Biochemistry, Alberta RNA Research and Training Institute, University of Lethbridge, Lethbridge, Alberta T1K 3M4, Canada

Little is known about the conservation of critical kinetic parameters and the mechanistic strategies of elongation factor (EF) Ts-catalyzed nucleotide exchange in EF-Tu in bacteria and particularly in clinically relevant pathogens. EF-Tu from the clinically relevant pathogen *Pseudomonas aeruginosa* shares over 84% sequence identity with the corresponding elongation factor from *Escherichia coli*. Interestingly, the functionally closely linked EF-Ts only shares 55% sequence identity. To identify any differences in the nucleotide binding properties, as well as in the EF-Ts-mediated nucleotide exchange reaction, we performed a comparative rapid kinetics and mutagenesis analysis of the nucleotide exchange mechanism for both the *E. coli* and *P. aeruginosa* systems, identifying helix 13 of EF-Ts as a previously unnoticed regulatory element in the nucleotide exchange mechanism with species-specific elements. Our findings support the base side-first entry of the nucleotide into the binding pocket of the EF-Tu·EF-Ts binary complex, followed by displacement of helix 13 and rapid binding of the phosphate side of the nucleotide, ultimately leading to the release of EF-Ts.

Elongation factor (EF)[2] Tu is an essential protein present in all kingdoms of life. It is among the most abundant proteins in any given cell, representing up to 5% of the total cellular protein in *Escherichia coli* (1). In its active GTP-bound state, EF-Tu delivers aminoacyl-tRNA (aa-tRNA) to actively translating ribosomes in a codon-dependent manner (2). EF-Tu·GTP has a high affinity for aa-tRNA ($K_D \approx 1 \times 10^{-8}$ M (3)) and forms a ternary complex that can interact with the ribosome (4). Correct codon-anticodon recognition greatly stabilizes the ternary complex on the ribosome and activates GTP hydrolysis. Following formation of GDP and subsequent P_i release (5, 6), EF-Tu undergoes a large conformational change (7, 8) causing the release of the bound aa-tRNA followed by accommodation of the aa-tRNA into the 50S ribosomal A site. The intrinsic rate of GDP dissociation from *E. coli* EF-Tu is extremely slow (0.002 s^{-1} (9)), requiring the guanine nucleotide exchange factor EF-Ts (10) to facilitate the rapid conversion of EF-Tu·GDP into its active GTP-bound state and to maintain rates of protein synthesis (~12 amino acids/s (11)) observed *in vivo*. Despite the critical cellular role of EF-Ts, its sequence is highly divergent among different bacterial species. Poor conservation of the primary sequence within bacterial EF-Ts sequences may give rise to differences in the enzymatic properties, raising the question of how and if the enzymatic properties are maintained among different bacterial EF-Tu·EF-Ts pairs. This is particularly interesting because the structure of the eukaryotic exchange factor is completely unrelated to its bacterial counterpart, whereas the respective structure for eEF1A remains similar to EF-Tu (12).

Based on the experimental approach used in previous studies to dissect the kinetic details of the interaction between EF-Tu, EF-Ts, and the functionally relevant nucleotides GDP and GTP (13–15) (Fig. 1), we performed a comparative mutational and rapid-kinetics analysis of the enzymatic properties of EF-Ts and EF-Tu from *E. coli* and the clinically relevant pathogen *Pseudomonas aeruginosa*. These two gram-negative bacterial species share 84 and 55% sequence identity between their respective EF-Tu and EF-Ts, enabling us to investigate the conservation of the overall enzymatic strategy for nucleotide exchange and the respective kinetic parameters among closely related species. In particular, it is interesting that EF-Ts from *P. aeruginosa* contains an extended C-terminal helix that interacts with a low conservation region on EF-Tu and that may play a functional role during nucleotide exchange.

Results

Nucleotide Binding Properties of P. aeruginosa EF-Tu (k_1, k_{-1}, k_5, and k_{-5})—Prior to a detailed investigation of the kinetic mechanism of *P. aeruginosa* EF-Ts mediated nucleotide exchange reaction, we first conducted a comparative analysis of the nucleotide binding properties of *P. aeruginosa* EF-Tu and *E. coli* EF-Tu. Rate constants for guanine nucleotide association and dissociation were determined using the stopped flow technique by measuring FRET between a single tryptophan in *P. aeruginosa* EF-Tu (Trp-40) or *E. coli* EF-Tu (Trp-184) and fluorescent methylanthraniloyl (mant)-labeled guanine nucleotides (13–15). Nucleotide dissociation rate constants were obtained in a chase experiment by mixing EF-Tu·mant-GTP/

* This work was supported by National Science and Engineering Research Council Operating Grant 326979-2011 (to H.-J. W.), Canada Foundation for Innovation Grant 202588 (to H.-J. W.), an Alberta Innovates Technology Futures New Investigator Award (to H.-J. W.), and Alberta Innovates Technology Futures postgraduate scholarships (to E. M.), as well as resource allocations by Compute Canada and Westgrid. The authors declare that they have no conflicts of interest with the contents of this article.

[1] To whom correspondence should be addressed: Dept. of Chemistry and Biochemistry, University of Lethbridge, 4401 University Dr., Lethbridge, Alberta T1K 3M4, Canada. Tel.: 403-329-2303; Fax: 403-329-2057; E-mail: hj.wieden@uleth.ca.

[2] The abbreviations used are: EF, elongation factor; aa-tRNA, aminoacyl-tRNA; mant, methylanthraniloyl; RMSF, root mean square fluctuation; MD, molecular dynamics.

GDP with excess unlabeled guanine nucleotide. Consistent with a first-order reaction, dissociation of guanine nucleotides from EF-Tu occurs with an observed single-exponential decay (Fig. 2, *A* and *B*). Rate constants (k_{-5} and k_{-1} for GTP and GDP) were directly obtained by fitting the observed time courses with a single-exponential function (Equation 1 under "Experimental Procedures") and are summarized in Table 1. Despite the high degree of sequence conservation between *P. aeruginosa* and *E. coli* EF-Tu, dissociation of GDP and GTP from *P. aeruginosa* EF-Tu ($k_{-1} = 0.0007 \pm 0.0001\ s^{-1}$, $k_{-5} = 0.007 \pm 0.001\ s^{-1}$) is slightly slower than from *E. coli* EF-Tu ($k_{-1} = 0.0018 \pm 0.0001\ s^{-1}$, $k_{-5} = 0.013 \pm 0.001\ s^{-1}$).

To determine the rate constants of GTP and GDP association, guanine nucleotide association was measured using a constant concentration of nucleotide-free EF-Tu and increasing concentrations of mant-GTP or mant-GDP (Fig. 2, *C* and *D*). The respective apparent rate constants (k_{app}) at different nucleotide concentrations were determined from the obtained fluorescence time courses by fitting with a single-exponential function (Equation 1). The linear dependence of k_{app} on the concentration of mant-GTP/mant-GDP was used to determine the respective association rate constants (k_5 and k_1) from the slope of the concentration dependence. The values for *P. aeruginosa* and *E. coli* EF-Tu are summarized in Table 1 and indicate a 3-fold faster rate of mant-GTP association (k_5) for *P. aeruginosa* EF-Tu but no difference in the mant-GDP association (k_1) rate constants. These rate constants reveal 5- and 2.8-fold higher affinities (K_d) of mant-GTP and mant-GDP for *P. aeruginosa* EF-Tu when compared with *E. coli* EF-Tu (summarized in Table 1).

EF-Ts-mediated Nucleotide Dissociation—To maintain *in vivo* rates of protein synthesis, EF-Ts is required to enhance the low intrinsic rate of guanine nucleotide dissociation from EF-Tu. This becomes even more relevant for *P. aeruginosa* EF-Tu with its tighter binding to nucleotides compared with *E. coli* EF-Tu. The interaction of EF-Tu·GTP or EF-Tu·GDP with EF-Ts can be described as two consecutive steps: the formation of the EF-Tu·nucleotide·EF-Ts ternary complex followed by the release of the bound guanine nucleotide (Fig. 1).

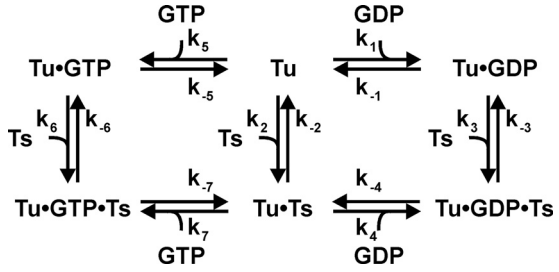

FIGURE 1. **Kinetic mechanism of nucleotide exchange in EF-Tu.**

TABLE 1
Kinetic parameters governing the nucleotide interaction with EF-Tu

	k_1 ($\mu M^{-1}\ s^{-1}$)[a]	k_{-1} (s^{-1})[b]	K_d (nM)[c]
EF-Tu(*E.coli*)	1.3 ± 0.1	0.0018 ± 0.0001	1.4 ± 0.1
EF-Tu(*P.aeruginosa*)	1.5 ± 0.1	0.0007 ± 0.0001	0.5 ± 0.1
	k_5 ($\mu M^{-1}\ s^{-1}$)[a]	k_{-5} (s^{-1})[b]	K_d (nM)[d]
EF-Tu(*E.coli*)	0.4 ± 0.1	0.013 ± 0.001	33 ± 9
EF-Tu(*P.aeruginosa*)	1.2 ± 0.1	0.007 ± 0.001	6 ± 1

[a] Association rate constants determined from slope of linear concentration dependence of k_{app}. The values are means ± S.D. of linear fitting.
[b] Dissociation rate constants determined in chase experiments.
[c] K_d calculated from k_{-1}/k_1.
[d] K_d calculated from k_{-5}/k_5.

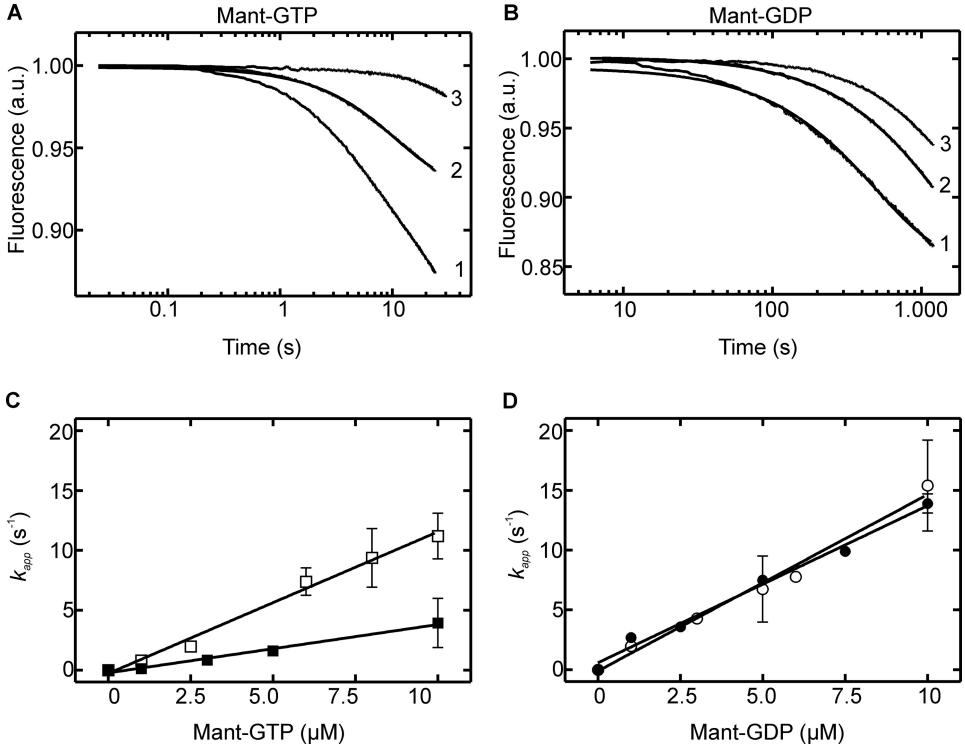

FIGURE 2. **Interaction of mant-GTP and mant-GDP with EF-Tu.** *A*, time course of *E. coli* EF-Tu·mant-GTP (0.3 μM) complex dissociation (*curve 1*), *P. aeruginosa* EF-Tu·mant-GTP (0.3 μM) complex dissociation (*curve 2*), and mant-GTP (3 μM) fluorescence over time (*curve 3*). *B*, time course of *E. coli* EF-Tu·mant-GDP (0.3 μM) complex dissociation (*curve 1*), *P. aeruginosa* EF-Tu·mant-GDP (0.3 μM) complex dissociation (*curve 2*), and mant-GDP (3 μM) alone (*curve 3*). *C*, concentration dependence of k_{app} values of mant-GTP binding to 0.3 μM *E. coli* EF-Tu (■) and 0.5 μM *P. aeruginosa* EF-Tu (□). *D*, concentration dependence of k_{app} values of mant-GDP binding to 0.3 μM *E. coli* EF-Tu (●) and 0.5 μM *P. aeruginosa* EF-Tu (○).

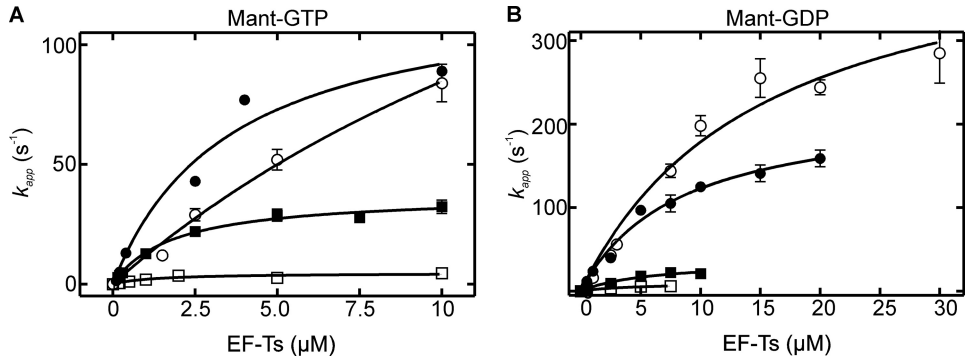

FIGURE 3. **Interaction of EF-Tu·GTP or EF-Tu·GDP and EF-Ts.** *A*, concentration dependence of k_{app} values of *E. coli* EF-Ts binding to *E. coli* EF-Tu·mant-GTP (●), *P. aeruginosa* EF-Ts binding to *E. coli* EF-Tu·mant-GTP (○), *P. aeruginosa* EF-Ts binding to *P. aeruginosa* EF-Tu·mant-GTP(■), and *E. coli* EF-Ts binding to *P. aeruginosa* EF-Tu·mant-GTP (□). *B*, concentration dependence of k_{app} values of *E. coli* EF-Ts binding to *E. coli* EF-Tu·mant-GDP (●), *P. aeruginosa* EF-Ts binding to *E. coli* EF-Tu·mant-GDP (○), *P. aeruginosa* EF-Ts binding to *P. aeruginosa* EF-Tu·mant-GDP (■), and *E. coli* EF-Ts binding to *P. aeruginosa* EF-Tu·mant-GDP (□). Components were mixed at the final concentrations in parentheses: EF-Tu·mant-GTP/GDP (0.3 μM) and EF-Ts (1–30 μM). The values are means ± S.D. from 5 to 15 time courses.

To study the EF-Ts-catalyzed dissociation of guanine nucleotides from EF-Tu, experiments were carried out using mant-GTP/mant-GDP. Upon mixing of the respective preformed EF-Tu·mant-nucleotide complexes with EF-Ts, a single exponential fluorescence decrease reflecting the mant-GTP/mant-GDP dissociation was observed. At low concentrations of EF-Ts, k_{app} increases linearly with the EF-Ts concentration, consistent with the formation of the EF-Tu·mant-GTP/mant-GDP·EF-Ts ternary complex. At high concentrations of EF-Ts, the rate of the reaction reaches saturation and equals the rate constant of nucleotide dissociation, *i.e.* k_{-7} (GTP) or k_{-4} (GDP) (Fig. 3). To assess the interchangeability of EF-Ts from either *E. coli* or *P. aeruginosa*, the experiment was also performed with EF-Tu·mant-GTP/mant-GDP from each species in the presence of EF-Ts from *E. coli* or *P. aeruginosa* (summarized in Tables 2 and 3). Consistent with previous reports, *E. coli* EF-Ts stimulates the dissociation of mant-GTP and mant-GDP from its EF-Tu more than 9,000-fold (k_{-7}/k_{-5}) and more than 130,000-fold (k_{-4}/k_{-1}), respectively. Similar to the *E. coli* system, mant-GTP and mant-GDP dissociation from *P. aeruginosa* EF-Tu is efficiently catalyzed by its own EF-Ts, more than 5000-fold (k_{-7}/k_{-5}) and 50,000-fold (k_{-4}/k_{-1}), respectively. However, dissociation of mant-GTP and mant-GDP from *P. aeruginosa* EF-Tu is accelerated only 700-fold (k_{-7}/k_{-5}) and 14,000-fold (k_{-4}/k_{-1}) by the *E. coli* exchange factor. In contrast to this, the *P. aeruginosa* exchange factor is able to stimulate the dissociation of mant-GTP and mant-GDP from *E. coli* EF-Tu more than 21,000-fold (k_{-7}/k_{-5}) and 270,000-fold (k_{-4}/k_{-1}), respectively.

It is surprising that *P. aeruginosa* EF-Ts is able to catalyze the dissociation of guanine nucleotides from *E. coli* EF-Tu more efficiently than the corresponding *E. coli* exchange factor. This is particularly astonishing because the interaction surface between EF-Tu and EF-Ts is highly conserved between the two species (Fig. 4*A*). The only exceptions to this are variations found within the C-terminal module (helix 13) of EF-Ts, pointing at a putative role for this helix during EF-Ts stimulated nucleotide dissociation from the EF-Tu·nucleotide·EF-Ts complex. The difference in sequence is subtle and includes a two-amino acid extension of helix 13 (Fig. 4*B*). The increased helix length and variation in its sequence might provide additional interactions between domain I of EF-Tu and helix 13 of *P. aeruginosa* EF-Ts that are not possible with the shorter *E. coli* helix.

TABLE 2
Rate constants for the kinetic mechanism of nucleotide exchange in *E. coli* EF-Tu

	k_2 (μM^{-1} s^{-1})[a]	k_{-2} (s^{-1})[b]	K_2 (nM)[c]
EF-Ts(*E.coli*)	19 ± 5	0.05 ± 0.04	3 ± 2
EF-Ts(*P.aeruginosa*)	5 ± 1	0.0006 ± 0.0002	0.12 ± 0.05
EF-Ts(Q283M)	10 ± 4	0.003 ± 0.002	0.3 ± 0.2
EF-Ts(Δ283)	3 ± 1	0.6 ± 0.3	200 ± 120
EF-Ts(Chimera)	20 ± 4	0.009 ± 0.001	0.5 ± 0.1
	k_3 (μM^{-1} s^{-1})[d]	k_{-3} (s^{-1})[e]	K_3 (μM)[f]
EF-Ts(*E.coli*)	60[m]	350[m]	5.8
EF-Ts(*P.aeruginosa*)	25 ± 2	150 ± 15	6 ± 1
EF-Ts(Q283M)	17 ± 1	33 ± 2	1.9 ± 0.2
EF-Ts(Δ283)	46 ± 12	2000 ± 500	43 ± 16
EF-Ts(Chimera)	32 ± 4	220 ± 35	7 ± 1
	k_4 (μM^{-1} s^{-1})[g]	k_{-4} (s^{-1})[h]	K_4 (μM)[i]
EF-Ts(*E.coli*)	14[m]	240 ± 20	17 ± 1
EF-Ts(*P.aeruginosa*)	3 ± 1	500 ± 100	167 ± 65
EF-Ts(Q283M)	10 ± 5	1000 ± 500	100 ± 71
EF-Ts(Δ283)	30 ± 10	30 ± 3	1.0 ± 0.3
EF-Ts(Chimera)	1.4 ± 0.4	380 ± 50	271 ± 85
	k_6 (μM^{-1} s^{-1})[d]	k_{-6} (s^{-1})[e]	K_6 (μM)[j]
EF-Ts(*E.coli*)	30[m]	60[m]	2
EF-Ts(*P.aeruginosa*)	9 ± 1	32 ± 14	4 ± 2
EF-Ts(Q283M)	17 ± 1	7 ± 1	0.4 ± 0.1
EF-Ts(Δ283)	40 ± 10	600 ± 100	15 ± 5
EF-Ts(Chimera)	50 ± 10	170 ± 50	3 ± 1
	k_7 (μM^{-1} s^{-1})[g]	k_{-7} (s^{-1})[h]	K_7 (μM)[k]
EF-Ts(*E.coli*)	6[m]	125 ± 20	21 ± 3
EF-Ts(*P.aeruginosa*)	0.4 ± 0.1	280 ± 90	700 ± 285
EF-Ts(Q283M)	13 ± 4	400 ± 100	31 ± 12
EF-Ts(Δ283)	0.28 ± 0.02	6 ± 1	21 ± 4
EF-Ts(Chimera)	0.24 ± 0.03	120 ± 20	500 ± 104

[a] Association rate constants determined from slope of linear concentration dependence of k_{app} on EF-Ts. The values are means ± S.D. of linear fitting.
[b] Dissociation rate constants calculated from all other rate constants. The values are means ± S.D. of GDP and GTP pathway.
[c] K_d calculated from k_{-2}/k_2.
[d] Association rate constants calculated from initial slope of linear concentration dependence of k_{app} on EF-Ts. The values are means ± S.D. of fitting.
[e] Dissociation rate constants determined from the plateau of k_{app} *versus* GDP. The values are means ± S.D. of fitting.
[f] K_d calculated from k_{-3}/k_3.
[g] Association rate constants calculated from initial slope of linear concentration dependence of k_{app} *versus* GDP. The values are means ± S.D. of fitting.
[h] Dissociation rate constants determined from the plateau of k_{app} *versus* EF-Ts. The values are means ± S.D. of fitting.
[i] K_d calculated from k_{-4}/k_4.
[j] K_d calculated from k_{-6}/k_6.
[k] K_d calculated from k_{-7}/k_7.
[m] Determined previously from Ref 9.

The Role of Helix 13 during Nucleotide Exchange—To dissect the role of helix 13 for the nucleotide exchange mechanism in EF-Tu, a C-terminal truncation variant, EF-Ts (Δ283), of *P. aeruginosa* EF-Ts (Fig. 4*B*) was constructed, and the kinetic

TABLE 3
Rate constants for the kinetic mechanism of nucleotide exchange in *P. aeruginosa* EF-Tu
The steps are as defined for Fig. 1.

Step	EF-Ts (*E. coli*)	EF-Ts (*P. aeruginosa*)	EF-Ts (Q283M)	EF-Ts (Δ283)	EF-Ts (chimera)
	s^{-1}	s^{-1}	s^{-1}	s^{-1}	s^{-1}
k_{-4}	10 ± 1	40 ± 10	>40	3 ± 1	>40
k_{-7}	5 ± 1	40 ± 2	190 ± 50	0.9 ± 0.1	25 ± 2

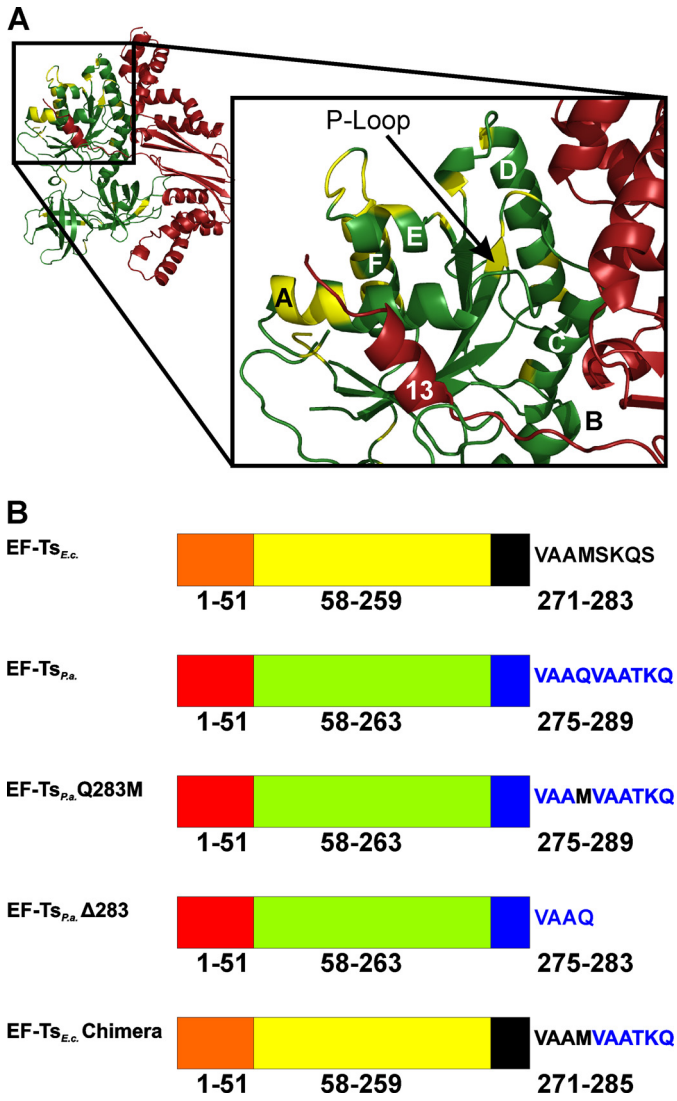

FIGURE 4. **EF-Ts variants.** *A*, structure and sequence conservation of EF-Tu and EF-Ts. The x-ray structure of the *E. coli* EF-Tu·EF-Ts complex (Protein Data Bank code 1EFU) shown in ribbon representation (EF-Tu in *green* and EF-Ts in *red*). *E. coli* EF-Tu helices are labeled with *capital letters*, and *E. coli* EF-Ts helices are labeled with *numbers* according to their succession from the N terminus to the C terminus of the protein. *Yellow* indicates positions in EF-Tu with non-conserved amino acids residues between the proteins from *E. coli* and *P. aeruginosa*. *B*, domain alignment of *E. coli* EF-Ts (N-terminal domain shown in *orange*, core domain in *yellow*, and the C-terminal domain in *black*) with *P. aeruginosa* EF-Ts (N-terminal domain shown in *red*, core domain in *green*, and the C-terminal domain in *blue*). Residue numbers for the domain boundaries are shown *below* the respective domains. The end of the C-terminal module sequence is shown on the *right*, and the name of each EF-Ts represented is given on the *left*. The substitution of Q283M is shown in the sequence (*P. aeruginosa* EF-Ts (Q283M)), highlighted in *black*. Residues corresponding to *P. aeruginosa* EF-Ts are denoted in *blue*, and residues corresponding to *E. coli* EF-Ts are denoted in *black*.

parameters describing the interactions between EF-Tu, the EF-Ts variants, and guanine nucleotides were determined using the approach described above (summarized in Table 3). Consistent with a role of the C-terminal extension of helix 13 during EF-Ts-mediated nucleotide dissociation, the C-terminal truncation variant of *P. aeruginosa* EF-Ts (EF-Ts(Δ283)) stimulated GTP and GDP dissociation from *P. aeruginosa* EF-Tu 44-fold (k_{-7}/k_{-7}) and 13-fold (k_{-4}/k_{-4}) less efficiently than wild type EF-Ts, respectively (Fig. 5 and Tables 2 and 3). A similar effect (47- and 16-fold for GTP and GDP, respectively) was also observed for EF-Ts(Δ283)-mediated nucleotide dissociation from *E. coli* EF-Tu. Similar to the *P. aeruginosa* system, the effect is strongest for GTP dissociation, suggesting that this is a common feature of the C-terminal extension present in *P. aeruginosa* EF-Ts. The conserved relative effect is particularly interesting because this EF-Ts is able to facilitate 6–10-fold faster GTP (k_{-7}/k_{-7}) and GDP (k_{-4}/k_{-4}) dissociation in *E. coli* EF-Tu then in its *P. aeruginosa* counterpart. Overall the *P. aeruginosa* EF-Ts-stimulated nucleotide dissociation from *E. coli* EF-Tu was twice as fast (k_{-7}/k_{-7} and k_{-4}/k_{-4}, respectively) as when stimulated by its own EF-Ts (Table 2). Thus, the C-terminal extension of helix 13 in EF-Ts from *P. aeruginosa* affects nucleotide dissociation from both its own EF-Tu and that of the *E. coli* to a similar extent, independent of the nucleotides present.

To further investigate the role of the C-terminal extension for the nucleotide exchange mechanism, we replaced the last four residues in *E. coli* EF-Ts (SKQS) with the last six residues (VAATKQ) from *P. aeruginosa*, constructing a chimera of EF-Ts (EF-Ts(Chimera); Fig. 4*B*). Interestingly, the dissociation rate constants describing EF-Ts(Chimera)-catalyzed mant-GTP/mant-GDP from *E. coli* EF-Tu are $k_{-7} = 120 \pm 20\ s^{-1}$ and $k_{-4} = 380 \pm 50\ s^{-1}$ (Table 2) and are similar to wild type *E. coli* EF-Ts. However, the EF-Ts(Chimera) reduces the association rate constants for mant-GTP/mant-GDP binding (k_7 and k_4, respectively) to the EF-Tu·EF-Ts complex 25- and 10-fold (Table 2). This effect is comparable with what we determined for k_7 and k_4 in the presence of *P. aeruginosa* EF-Ts (15- and 5-fold reduction, respectively), suggesting a role of the C-terminal helix in modulating the nucleotide association kinetics. Ultimately, given the unchanged dissociation rate constant, replacing the C-terminal residues in *E. coli* EF-Ts with those from *P. aeruginosa* lowers the nucleotide affinity for mant-GTP/mant-GDP (K_7 and K_4) to the EF-Tu·EF-Ts complex 24- and 16-fold, making it similar to the affinity for the *E. coli* EF-Tu *P. aeruginosa* EF-Ts complex (Table 2). This is consistent with the fact that the EF-Ts(Chimera) is able to catalyze dissociation of mant-GTP/mant-GDP from *P. aeruginosa* EF-Tu more like the EF-Ts from *P. aeruginosa* (Table 3), despite the fact that 98% of its sequence is identical to *E. coli* EF-Ts.

When comparing the interactions of the helix 13 residues in the structure of the EF-Tu·EF-Ts complex from *E. coli* (16) with

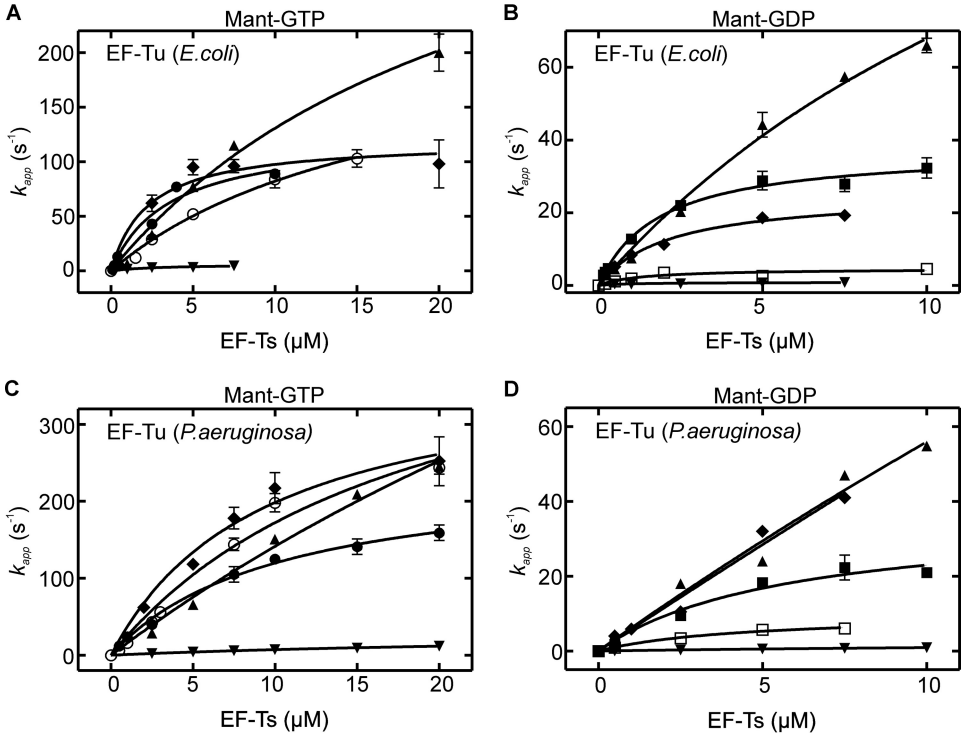

FIGURE 5. **EF-Ts catalyzed dissociation of guanine nucleotides.** Concentration dependence of mant-GTP (*A*) and mant-GDP dissociation (*B*) from *E. coli*, as well as from *P. aeruginosa* (*C* and *D*, respectively) EF-Tu (final concentration, 0.3 μM) stimulated by increasing concentrations of *E. coli* EF-Ts (●), *P. aeruginosa* EF-Ts (○), EF-Ts(Δ283) (▼), EF-Ts(Q283M) (▲), and EF-Ts(Chimera) (♦). Apparent rate constants were obtained from individual fluorescence time courses by single-exponential fitting. The values indicated are means ± S.D. from 5 to 15 time courses.

the sequence of the *P. aeruginosa* factors, we observed that Met-278 within helix 13 of *E. coli* EF-Ts makes a number of hydrophobic contacts with Ala-29 and Thr-25 located close to the magnesium ion binding site in domain I of EF-Tu (16). These interactions might promote nucleotide binding through supporting the coordination of the magnesium ion by Thr-25. We therefore substituted Gln-283 in *P. aeruginosa* EF-Ts (which is the corresponding residue to *E. coli* Met-278) with Met (EF-Ts (Q283M); Fig. 4*B*). This substitution resulted in only slightly increased nucleotide dissociation rate constants for *P. aeruginosa* EF-Tu (Fig. 4*B* and Table 2 and 3). Interestingly, the nucleotide association was 3-fold (k_4) faster for mant-GDP and 32-fold faster (k_7) for mant-GTP (Table 2). Therefore, the substitution of Gln-283 mainly affects the association step and is most pronounced for GTP.

The Role of Helix 13 for Ternary Complex Stability—To determine whether helix 13 has a mechanistic role in the dissociation of EF-Ts from the EF-Tu·GTP/GDP·EF-Ts complex, a GTP/GDP titration against a fixed concentration of purified EF-Tu·EF-Ts complexes was performed similar to previous studies (13–15). The observed change in the intrinsic tryptophan fluorescence of EF-Tu reflects the dissociation of EF-Ts from the transiently formed EF-Tu·GTP/GDP·EF-Ts complex. The rates of EF-Ts dissociation were determined from time courses using a single-exponential fit and plotted as a function of increasing guanine nucleotide concentration (Fig. 6). At saturating concentrations of guanine nucleotide, where rebinding of EF-Ts is negligible and EF-Ts dissociation is not limited by guanine nucleotide binding, the rate constants for EF-Ts dissociating from the EF-Tu·GTP/GDP·EF-Ts ternary complex (k_{-6} and k_{-3}) can be determined (Fig. 1 and Table 2). From the slope of the concentration dependence, the corresponding association rate constants (k_6 and k_3) can be calculated (9). The location of the tryptophan residue within *P. aeruginosa* EF-Tu did not allow for a detectable change in the tryptophan signal upon GDP-induced dissociation of the Tu·Ts complex. Therefore, k_{-3}, k_3, and k_4 could not be determined for the respective *P. aeruginosa* EF-Tu-containing complexes.

Using *E. coli* EF-Tu, we were able to compare the rate constants for dissociation of *P. aeruginosa* and *E. coli* EF-Ts from ternary EF-Tu·nucleotide·EF-Ts complexes. For both EF-Tu·GTP·EF-Ts and EF-Tu·GDP·EF-Ts complexes, the rates of EF-Ts dissociation (k_{-6} and k_{-3}) were 2-fold slower than *E. coli* EF-Ts. A similar 2–3-fold (k_3 and k_6) effect was observed for the association rate constants for the binding of *P. aeruginosa* EF-Ts to both *E. coli* EF-Tu·GDP and EF-Tu·GTP (Table 2). Interestingly, the removal of the C-terminal extension in *P. aeruginosa* EF-Ts, EF-Ts(Δ283), increases the rate constants for dissociation from the GTP and GDP-complexes 19- and 13-fold (k_{-6} and k_{-3}), respectively. When compared with wild type *E. coli* EF-Ts, the rate constants are 10- and 6-fold faster. These effects on the dissociation rate constants are stronger than for the association rate constants, where a 4-fold increase (k_6) in association rate constant for the *P. aeruginosa* EF-Ts binding to *E. coli* EF-Tu·GTP suggests a role for helix 13 in the interaction with the GTP conformation of EF-Tu. Surprisingly, grafting the C-terminal six amino acid residues from *P. aeruginosa* on EF-Ts from *E. coli* has no effect on either the association or dissociation rate constants to the GTP (k_6 and k_{-6}) or GDP (k_3 and k_{-3}) conformation of *E. coli* EF-Tu (Table 2).

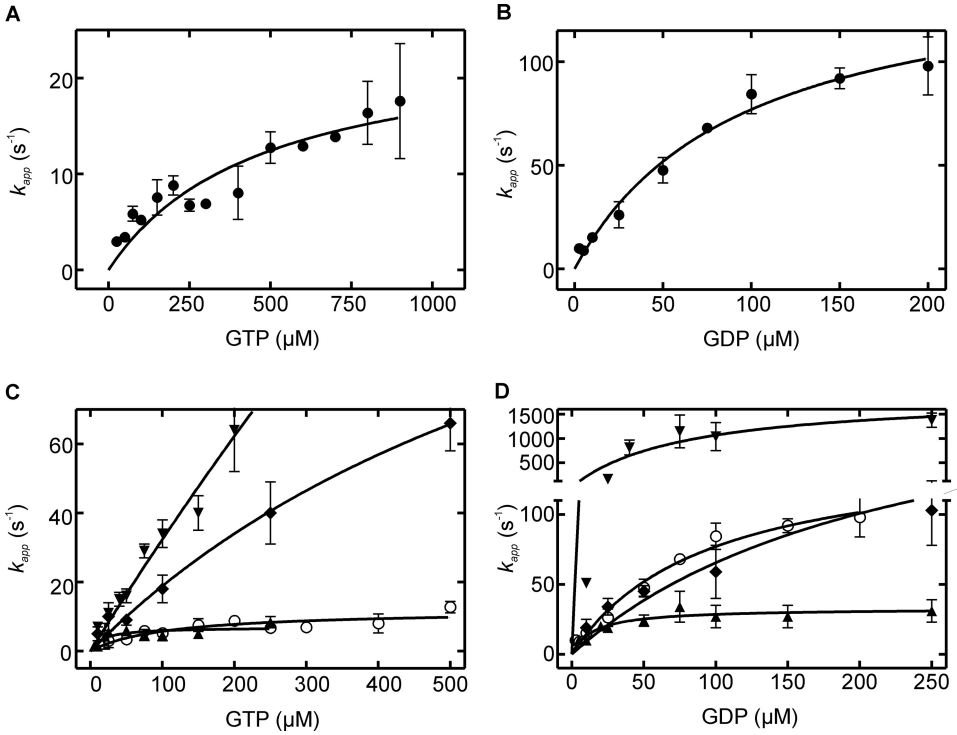

FIGURE 6. **Nucleotide-induced dissociation of EF-Tu·EF-Ts complexes.** *A* and *B*, GTP (*A*) and GDP (*B*) concentration dependence of k_{app} for EF-Tu·EF-Ts (0.5 μM) complex dissociation containing *E. coli* EF-Ts (●), as well as GTP (*C*) and GDP (*D*) dependence of k_{app} for EF-Tu·EF-Ts (0.5 μM) complex dissociation containing *P. aeruginosa* EF-Ts (○), EF-Ts(Δ283) (▼), EF-Ts(Q283M) (▲), or EF-Ts(Chimera) (◆). Apparent rate constants were obtained from individual fluorescence time courses by single-exponential fitting. The values are means ± S.D. from 5 to 15 time courses.

However, substitution of Gln-283 with Met reduces the rate constant of *P. aeruginosa* EF-Ts dissociation from the EF-Tu·GTP·EF-Ts complex 5-fold (k_{-6}) and increases the rate constant for binding 2-fold (k_6), which results in a 10-fold increased affinity (K_6) of EF-Ts(Q283M) to the *E. coli* EF-Tu·GTP complex. A similar 5-fold (k_{-3}) decrease in the dissociation rate constant is also observed for the GDP containing ternary complex, which is accompanied by a small 1.5-fold (k_3) reduction in the association rate constant. Based on this, the affinity of EF-Ts(Q283M) for the GDP-bound *E. coli* EF-Tu is affected in the similar direction by this single amino acid substitution in helix 13 but is less pronounced than for the GTP-containing complex and only 3-fold (K_3) higher than wild type *P. aeruginosa* EF-Ts.

The Role of Helix 13 for EF-Tu·EF-Ts Binary Complex Stability—To investigate how the effects of altered C-terminal sequences in EF-Ts relate to the formation of the nucleotide-free binary EF-Tu·EF-Ts complex, we used the same approach as above monitoring the change of the intrinsic tryptophan fluorescence of *E. coli* EF-Tu (Fig. 7). The obtained values for k_2 and k_{-2} are summarized in Table 2. In agreement with previously published data (9), k_2 for the EF-Tu and EF-Ts complex from *E. coli* is 19 ± 5 × 10^6 M^{-1} s^{-1}. On the other hand, the association rate constant for *E. coli* EF-Tu and EF-Ts from *P. aeruginosa* is slightly reduced (3.8-fold). The dissociation rate constant (k_{-2}) for the EF-Tu·EF-Ts complexes can be calculated from the remaining rate constants in the kinetic mechanism (9, 15). Interestingly, k_{-2} for the *E. coli* EF-Tu·EF-Ts and the complex containing *E. coli* EF-Tu and EF-Ts from *P. aeruginosa* were 0.05 ± 0.04 s^{-1} and 0.0006 ± 0.0002 s^{-1}, respectively (Table 2). This results in an affinity (K_2) for the mixed *E. coli*/*P. aeruginosa* complex of 0.12 nM, which is 25-fold higher than for the *E. coli* EF-Tu·EF-Ts complex (K_2 = 3 nM). Consistent with a role of the C-terminal extension in increasing the affinity of EF-Ts for EF-Tu, removing the last six amino acids from *P. aeruginosa* EF-Tu (K_2 = 200 nM) reduces the affinity 1600-fold. This is mainly due to a 1000-fold increased dissociation rate constant (k_{-2}) without a change in the corresponding association rate constant (Table 2). This trend is continued in the EF-Ts variant containing the last six amino acids of *P. aeruginosa* EF-Ts. Although the effect is less pronounced, the affinity of the EF-Ts(Chimera) to EF-Tu from *E. coli* is still 6-fold higher (K_2) than wild type *E. coli* EF-Ts, mainly because of a 6-fold (k_{-2}) decreased dissociation rate constant. Interestingly, the identity of the amino acid in position 283 of *P. aeruginosa* EF-Ts is not responsible for this effect, because this substitution variant has only a 2-fold lower (K_2) affinity than wild type EF-Ts from *P. aeruginosa*.

Molecular Dynamics Simulations Reveal Destabilization of Helix F in EF-Tu by EF-Ts—Based on our kinetic analysis above, it is evident that the C-terminal module of EF-Ts (helix 13) strongly modulates the interaction between EF-Tu and guanine nucleotides. To obtain a structural understanding of this effect, all-atoms models of *E. coli* EF-Tu·EF-Ts and EF-Tu·EF-Ts (Chimera) were constructed and simulated using molecular dynamics similar to our previous studies (15, 17, 18). After constructing a model of the EF-Tu·EF-Ts(Chimera) complex, the C terminus of EF-Ts(Chimera) was subjected to simulated annealing to investigate which regions of EF-Tu it may interact with. Based on 20 independent annealing simulations, the

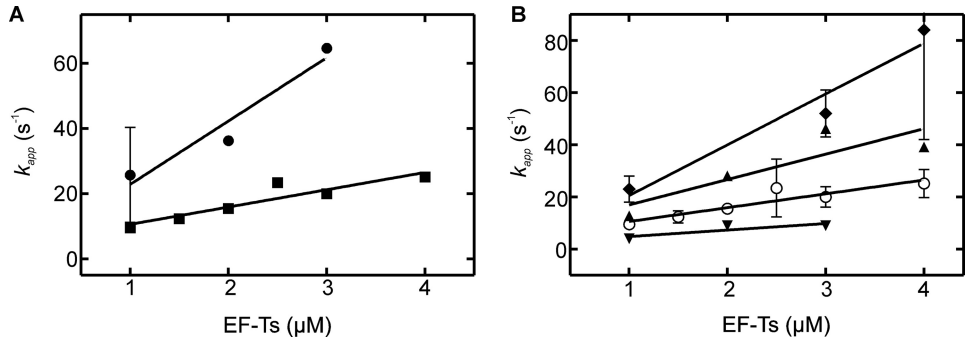

FIGURE 7. **EF-Tu·EF-Ts interactions.** Concentration dependence of the rate of EF-Tu·EF-Ts complex formation measured as fluorescence changes of Trp-184 in *E. coli* EF-Tu upon addition of *E. coli* EF-Ts (●) or *P. aeruginosa* EF-Ts (■) (*A*) and for *P. aeruginosa* EF-Ts (○), EF-Ts(Δ283) (▼), EF-Ts(Q283M) (▲), and EF-Ts(Chimera) (♦) (*B*). The rates were obtained by exponential fitting of single fluorescence time courses observed after rapid mixing of equal volumes of EF-Tu (1 μM) and EF-Ts containing solutions (means ± S.D. from 5 to 15 time courses).

C-terminal module of EF-Ts(Chimera) likely contacts EF-Tu either at the switch I region or helix F (near the base-side interactions of the nucleotide-binding pocket; Fig. 4*A*). Evidence suggests, however, that the switch I region of EF-Tu is disordered when bound to EF-Ts (16). Thus, differences in the structural dynamics between *E. coli* EF-Tu·EF-Ts and EF-Tu·EF-Ts(Chimera) complexes that can account for the observed differences in nucleotide interaction *in vitro* likely originate in the helix F region (Fig. 4*A*).

The MD simulations of these models were stable after 5 ns based on backbone root mean square deviation and root mean square fluctuation (RMSF) calculations (Fig. 8, *A* and *B*), and the overall dynamics of the complexes are largely similar (Fig. 8*B*). Throughout both simulations the C-terminal helix of EF-Ts remains in contact with the G-domain of EF-Tu. Interestingly, the amino acids following the C-terminal helix of EF-Ts show different dynamics in the *E. coli* EF-Tu·EF-Ts and EF-Tu·EF-Ts(Chimera) simulations. In the *E. coli* EF-Tu·EF-Ts complex, the three C-terminal amino acids (280–282) pack against the G-domain of EF-Tu (Fig. 9, *A* and *C*). In the EF-Tu·EF-Ts(Chimera) simulation, however, the five C-terminal amino acids (280–284) exhibit higher mobility and do not pack efficiently on EF-Tu (Fig. 9, *B* and *D*). This difference in the C termini of *E. coli* EF-Ts and EF-Ts(Chimera) is correlated with the stability of a nearby hydrogen-bonding network (Lys-37/Glu-185/Asp-181) in EF-Tu (Fig. 9, *C* and *D*).

In *E. coli* EF-Tu·EF-Ts, the C-terminal amino acids of EF-Ts form hydrophobic interactions with the side chain of Lys-37, which appears to stabilize the hydrogen bond network formed by Lys-37, Glu-185, and Asp-181 (Fig. 9). Because the C-terminal amino acids in EF-Ts(Chimera) are mobile, they do not form the same hydrophobic interactions, and the resulting increase in mobility of the Lys-37 side chain destabilizes the Lys-37/Glu-185/Asp-181 hydrogen bonding network (Fig. 9). In quantitative terms, the hydrogen bond between Glu-185 and Asp-181 in helix F of EF-Tu is stable throughout the entire simulation of the *E. coli* EF-Tu·EF-Ts complex but only for 75% of the simulation of EF-Tu·EF-Ts(Chimera) (Fig. 10*A*).

To investigate how the differential stabilities of this hydrogen-bonding network affect the structural dynamics of the complex, the Φ and Ψ angles for each amino acid in EF-Tu were plotted as a "Ramachandran histogram" (17). This analysis revealed highly flexible amino acids as those that occupied multiple conformations. Interestingly, the loop connecting helix E and helix F (Fig. 4*A*) in EF-Tu (Gly-180, Asp-181, and Ala-183) was found to be more flexible when bound to EF-Ts(Chimera) compared with *E. coli* EF-Ts (Fig. 10*B*). Because the N terminus of helix E interacts with the guanine base of the bound nucleotide, backbone destabilization of the loop between helix E and F may ultimately destabilize bound nucleotides. Taken together, our *in vitro* and *in silico* results suggest that the C terminus of EF-Ts(Chimera) destabilizes the loop between helixes E and F in EF-Tu, which compromises interactions between bound nucleotides and helix E, thus increasing the rates of nucleotide dissociation.

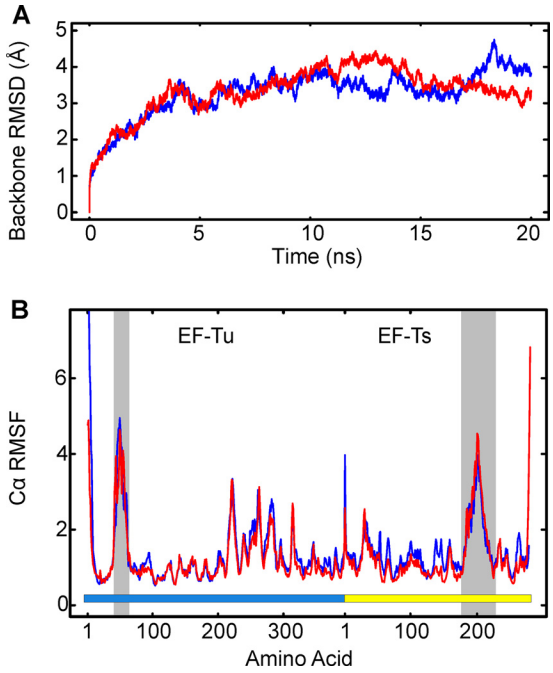

FIGURE 8. **Molecular dynamics simulations.** *A*, stability of molecular dynamics simulations of *E. coli* EF-Tu·EF-Ts and the *E. coli* complex containing EF-Ts(Chimera). The root mean square deviation was computed for the non-hydrogen backbone atoms of EF-Tu·EF-Ts (*blue*) and EF-Tu·EF-Ts(Chimera) (*red*) models during 20-ns MD simulations. *B*, the overall dynamics of EF-Tu·EF-Ts and EF-Tu·EF-Ts(Chimera) are similar in MD simulations. The RMSF of each Cα atom was measured every 2 ps from 10 to 20 ns of MD simulation. The RMSF is plotted as a function of amino acid for EF-Tu·EF-Ts (*blue*) and EF-Tu·EF-Ts(Chimera) (*red*). The *shaded regions* indicate the switch I region of EF-Tu and helices 10 and 11 of EF-Ts from *left* to *right*, respectively. The *colored bar* indicates EF-Tu (*blue*) and EF-Ts (*yellow*) as they are shown in Fig. 9.

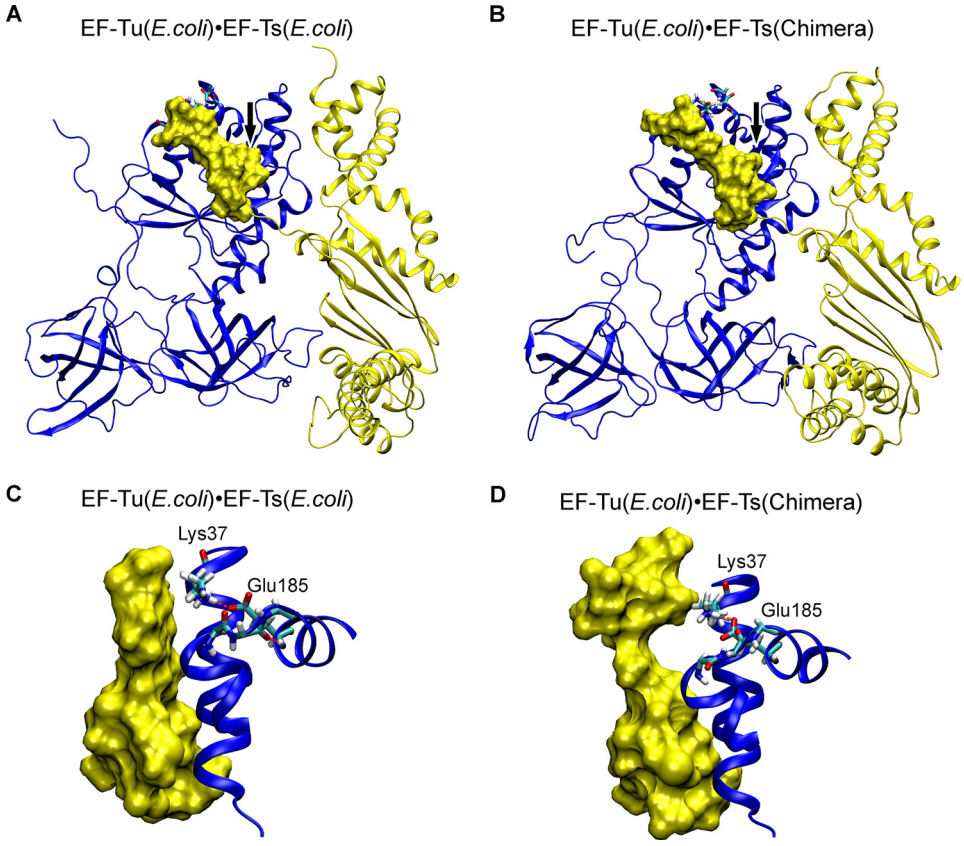

FIGURE 9. **Helix 13 of EF-Ts(Chimera) interacts differently with the G domain of EF-Tu than *E. coli* EF-Ts.** Snapshots of the EF-Tu·EF-Ts complexes were taken after 20 ns of MD simulation for *E. coli* EF-Tu·EF-Ts (*A*) and EF-Tu·EF-Ts(Chimera) models (*B*). *C* and *D* are close-ups of *A* and *B*, respectively, rotated by ~90°. EF-Tu is colored *blue*, and EF-Ts is colored *yellow*. The C terminus of EF-Ts (from position 271 to the end) is represented as a surface. Amino acids Lys-27 and Glu-185, as well as the backbone atoms of amino acids Gly-180, Asp-181, and Ala-182 of EF-Tu are shown as *sticks*. Hydrogen bonds are represented as *red dashed lines*. The *arrows* in *A* and *B* indicate the location of the nucleotide-binding pocket in EF-Tu.

Discussion

Guanine Nucleotide Exchange in E. coli and P. aeruginosa EF-Tu—Kinetic parameters describing the interaction of the essential elongation factor Tu with guanine nucleotides are available for a number of different model systems, such as yeast and *E. coli*, revealing large functionally relevant differences in affinities (9, 19, 20). However, little is known about the conservation of these fundamental and functionally critical parameters in bacteria, particularly in clinically relevant pathogens such as *P. aeruginosa*. The rapid kinetics analysis performed here, comparing the nucleotide binding properties of EF-Tu from *E. coli* and *P. aeruginosa*, revealed that EF-Tu from *P. aeruginosa* binds GDP with subnanomolar and GTP with low nanomolar affinity. Compared with the well established parameters for *E. coli* (9, 15), the affinity is 3–5-fold higher for GDP and GTP, respectively. This effect is mainly due to a decreased rate constant for dissociation of the nucleotide from the factor, suggesting either that the nucleotide-bound state has lower energy than the corresponding *E. coli* complex or that the transition state energy is higher. Either way, this will have implications for the mechanistic strategies employed by the nucleotide release factor. Interestingly, the EF-Ts stimulated release of GTP or GDP is also 3– 6-fold slower than in *E. coli*. Nevertheless, the strategy to equalize the dissociation rates for GTP and GDP (9) is maintained, as well as the 10-fold difference in dissociation rate of the nucleotide from the respective EF-Tu·nucleotide complex (9).

The high degree of sequence conservation between the two EF-Tu (84%, data not shown) raises questions regarding the structural and sequence origins of the observed differences in the nucleotide binding properties and how the *P. aeruginosa* EF-Ts is able to overcome them. Mapping the sequence differences between the two species onto the structure of the EF-Tu·EF-Ts complex from *E. coli* reveals that in addition to the conserved interactions between domains 1 and 3 of EF-Tu and EF-Ts, helix 13 of EF-Ts contains an extension that maps to a region on the surface of EF-Tu corresponding to helix F and E. Interestingly, this region contains the highest number of non-conserved residues between EF-Tu from *E. coli* and *P. aeruginosa* (Fig. 4*A*). A functional role of this interaction for fine-tuning the nucleotide binding properties in the EF-Tu·EF-Ts pair is consistent with our observation that removal of this region of the helix has a strong effect (16 to 44-fold decrease) not only on the EF-Ts stimulated nucleotide dissociation from *P. aeruginosa* EF-Tu but also from *E. coli*. This is in line with previous work that found that removal of the whole helix 13 affects nucleotide release (21). However, this study removed the helix completely, whereas in our work, only the C-terminal six amino acids were removed, pointing to a mechanistic role of this particular region in helix 13. Furthermore, the fact that the

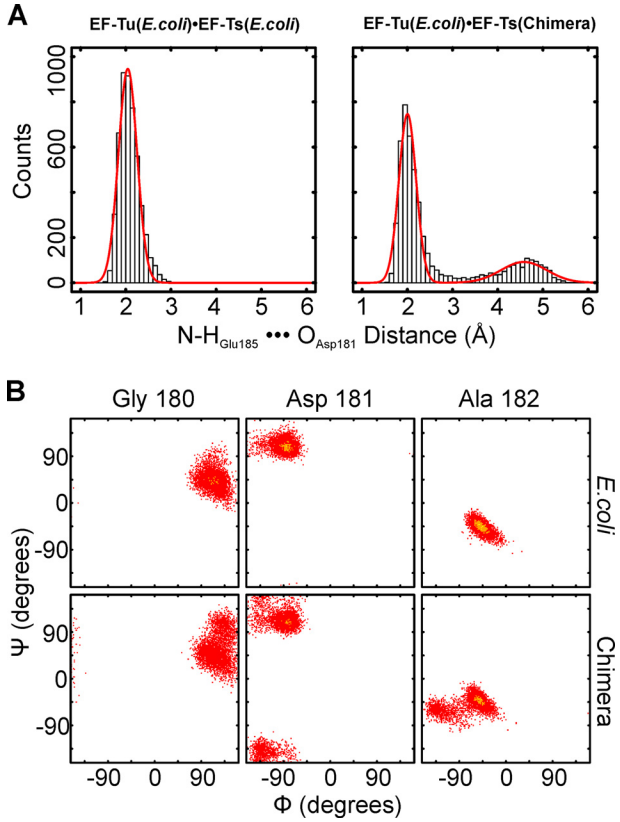

FIGURE 10. **The N terminus of Helix F in EF-Tu exhibits increased structural dynamics when interacting with helix 13 of EF-Ts(Chimera).** *A*, hydrogen bond distances were measured between the backbone atoms of Glu-185 and Asp-181 at the N terminus of helix F of EF-Tu in MD simulations of *E. coli* EF-Tu·EF-Ts and EF-Tu·EF-Ts(Chimera) and plotted as histograms. The *red lines* are fits to single (*left*) and double (*right*) Gaussian functions, demonstrating that the N-H(Glu-185) ··· O(Asp-181) hydrogen bond is only present in 76% of the analyzed frames for EF-Tu·EF-Ts(Chimera) compared with EF-Tu·EF-Ts. *B*, backbone dihedral angles were measured in MD simulations of *E. coli* EF-Tu·EF-Ts (*top*) and EF-Tu·EF-Ts(Chimera) (*bottom*). The values for each amino acid were plotted as a two-dimensional histogram of Φ *versus* Ψ. Each histogram is divided into bins with dimensions $\pi/32 \times \pi/32$. Each bin was colored based on the occupancy from *red* (low occupancy) to *yellow* (high occupancy).

effect occurs in *E. coli* EF-Tu, as well as *P. aeruginosa* indicates that this mechanistic strategy is likely common in bacteria. This transferability is further supported by the effect of transplanting these six residues from *P. aeruginosa* EF-Ts onto *E. coli* EF-Ts. Notably, this chimera has the ability to increase the rate of EF-Ts stimulated nucleotide release using the *E. coli* exchange factor scaffold to the level observed for the *P. aeruginosa* factor, a surprising result given the low overall sequence conservation of the factors (55%, data not shown).

A more detailed mechanistic understanding of the role of the C-terminal segment of helix 13 during stimulated nucleotide release can be derived from the kinetic parameters describing the interaction in the heterologous system containing EF-Tu from *E. coli* and EF-Ts from *P. aeruginosa*. Here the *P. aeruginosa* EF-Ts performs as a "super" nucleotide release factor because it is able to catalyze nucleotide release more efficiently than the *E. coli* exchange factor, lowering the nucleotide affinity an additional 10-fold (K_4) for GDP and over 30-fold (K_7) for GTP. This additional destabilization of nucleotide binding is mainly achieved by destabilizing binding of the nucleotide to the EF-Tu·EF-Ts binary complex accompanied by a slight increase in the rate of nucleotide dissociation (Table 2). Reduction in the nucleotide association rate constant is more pronounced for GTP than for GDP. This effect can be attributed to the last six amino acids in helix 13 of EF-Ts, because the EF-Ts chimera contains just these residues from *P. aeruginosa* in an otherwise *E. coli* sequence background. This six-residue substitution essentially turns *E. coli* EF-Ts into a *P. aeruginosa* EF-Ts from a kinetics point of view. Interestingly, this effect does not have a nucleotide preference and does not involve nucleotide dissociation. Together with the structural dynamics data obtained from our MD simulations of the EF-Tu·EF-Ts(Chimera) binary complex, this suggests a model where the C-terminal end of helix 13 of EF-Ts interacts with helices E and F in EF-Tu, destabilizing the structure and increasing the flexibility of helix E. Because the N-terminal end of helix E is involved in nucleotide binding through hydrogen bonding of Ser-173 with the carbonyl oxygen of the nucleobase, this should ultimately lead to decreasing the nucleotide-binding energy. This is supported by our kinetic data showing 10- and 20-fold (k_7) reductions in the nucleotide association (GDP and GTP) rate when comparing EF-Ts (Chimera) with wild type EF-Ts. A functionally relevant interaction network between helix 13 in the region of helix F and E is further supported by the observation that removal of the C-terminal extension selectively increases EF-Ts dissociation from EF-Tu. This suggests that the incoming nucleotide, when bound to the base-side of the binding pocket on EF-Tu, will stabilize the structural dynamics of the F-E helix network. In turn, this will induce dissociation of helix 13 from this region, which then is followed by disruption of the interaction that the N-terminal end of helix 13 makes with helix A and the phosphate side of the nucleotide-binding pocket (Fig. 4*A*).

Our observations lead to a model that supports the base side-first entry of the nucleotide into the binding pocket of the EF-Tu·EF-Ts binary complex, which will be followed by displacement of helix 13 and rapid binding of the phosphate side of the nucleotide, ultimately leading to the release of EF-Ts (Fig. 11). This model is consistent with SMD simulations inducing nucleotide dissociation via extraction of the phosphate side that shows the junction between helix F and helix E as highly flexible (17). It also provides a strategy for efficient discrimination between different nucleotides (adenine *versus* guanine), because these base side interactions must occur prior to complete accommodation of the nucleotide and the subsequent stabilization of binding by interactions with the nucleotide phosphates, which are energetically different for the di- and triphosphate forms. This ultimately allows the EF-Tu·EF-Ts complex to effectively screen the identity of the incoming nucleotide. Our findings demonstrate that the overall strategy for nucleotide exchange is likely conserved among different bacterial species and that alterations in the individual sequences and enzymatic properties of EF-Tu and EF-Ts seem to have evolved to compensate and to maintain the overall catalytic strategy of equalizing the dissociation rates (k_{-4} and k_{-7}) for the nucleotide, maintaining a rate that is almost 10 times faster than the protein synthesis rate. Furthermore, the role of helix 13 identified here might explain how the corresponding structurally unrelated eukaryotic nucleotide exchange factor

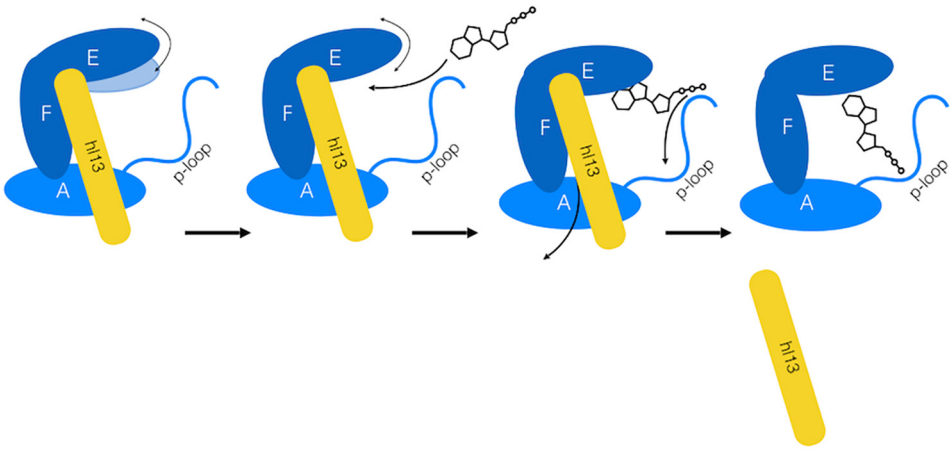

FIGURE 11. **Molecular mechanism of nucleotide base side-first entry into the EF-Tu·EF-Ts binding pocket followed by helix 13 displacement.** The C-terminal end of helix 13 of the EF-Ts interacts with helices E and F, destabilizing the structure and increasing the flexibility of helix E. Base side-first entry of the nucleotide into the binding pocket allows for selection of the nucleotide by stabilization of the helix F-E network in the presence of guanine nucleotides, inducing dissociation of helix 13 and rapid binding of the phosphate side of the nucleotide leading to the release of EF-Ts.

has evolved as helix 13 and eEF1Bα approach the nucleotide-binding pocket from the same side (12).

In summary, we report for the first time that the nucleotide binding properties of EF-Tu vary even between closely related bacterial species, that nucleotide binding occurs via the base side-first entry into the nucleotide-binding pocket, and that fine-tuning of the initial base side entry kinetics via modulation of the structural dynamics of the respective side of the EF-Tu nucleotide-binding pocket by helix 13 of EF-Ts is the strategy used by bacterial EF-Ts to adjust for nucleotide binding affinity differences.

Experimental Procedures

Molecular Biology—All restriction enzymes used were purchased from Fermentas, and primers were obtained from Integrated DNA Technologies. For the recombinant expression of *E. coli* EF-Tu and EF-Ts, the previously reported constructs pKECAHIS (22), pCA24N*tsf* (23), and pHK1Ts (13) were used.

Cloning of P. aeruginosa tufA and tsf—The EF-Tu encoding *tufA* gene was PCR-amplified from *P. aeruginosa* genomic DNA using Phusion polymerase (Finnzymes) utilizing the primers 5′-AGA GGA TCC CTG TCG TGG CTA AAG GA-3′ and 5′-ATG GCA GGA GCT CCG ATT ACT CGA-3′, introducing BamHI and SacI restriction sites (underlined). In a similar fashion the *tsf* gene coding for EF-Ts was amplified from *P. aeruginosa* genomic DNA, using the primers 5′-TTC CAT ATG GCA GAA ATT ACT GCA GC-3′ and 5′-CAG TCG AAT TCG TCT TTG TTA CTG-3′, with engineered NdeI and EcoRI restriction sites, respectively. The resulting PCR products were ligated into SmaI-digested pUC19 (New England BioLabs) using T4 DNA ligase (Invitrogen). The ligation mixture was transformed into subcloning efficiency *E. coli* DH5α cells (New England BioLabs). The resulting pUC19 constructs were digested with restriction enzymes corresponding to the recognition sequence introduced via the respective PCR primers. The resulting insert fragments were then ligated (T4 DNA ligase) into similarly digested pET28a to yield pET28*tuf*Pa and pET28*tsf*Pa. Sequence and orientation was confirmed by DNA sequencing (Macrogen DNA Sequencing Services).

Mutagenesis—The single amino acid substitution variant of *P. aeruginosa* EF-Ts (Q283M) was generated via site-directed mutagenesis using the QuikChange™ method (Stratagene). The QuikChange™ method was also used for construction of the *P. aeruginosa* EF-Ts C-terminal deletion variant, EF-Ts(Δ283), by introducing a stop codon in position 283, as well as construction of the *E. coli* EF-Ts(Chimera) containing the last six amino acids of the *P. aeruginosa* EF-Ts. (EF-Ts(Q283M): forward primer, 5′-GCT GCT GAA GTT GCC GCT **ATG** GTA GCC GCC ACC AAG C-3′, and reverse primer, 5′-GCT TGG TGG CGG CTA C**CA** **T**AG CGG CAA CTT CAG CAG C-3′; EF-Ts(Δ283): forward primer, 5′-GCC GCT CAA **TAA** GCT TCC ACC AAG C-3′, and reverse primer, 5′-GCT TGG TGG AAG C**TT** **A**TT GAG CGG C-3′; and EF-Ts(Chimera): forward primer, 5′-GTT GCT GCC ATG **GTA GCC GCC ACC AAG CAG** TGC TTT GCC AAG G-3′, and reverse primer, 5′-CCT TGG CAA AGC A**CT GCT TGG TGG CGG CTA C**CA TGG CAG CAA C-3′). The positions of the respective mutations are given in bold type, and underlined nucleotides denote the restriction sites inserted via silent mutations used for screening (AcuI, HindIII, and NcoI, respectively). The resulting amplification products were transformed into *E. coli* DH5α (New England Biolabs) competent cells for propagation. The mutations were confirmed by sequencing (GeneWiz Inc.).

Protein Expression and Purification—EF-Tu and EF-Ts variants derived from *P. aeruginosa* were expressed in *E. coli* BL21-DE3 (Novagen) containing the respective plasmid. The cells were grown at 37 °C in LB medium supplemented with 50 μg/ml kanamycin to the mid-log phase (A_{600} = 0.6) and induced with 1 mM isopropyl thio-β-galactoside (BioBasic). The cells were grown for an additional 3 h at 37 °C, harvested by centrifugation (5000 × *g* for 10 min at 4 °C), and stored at −80 °C.

EF-Tu from *E. coli* was expressed in LB supplemented with 100 μg/ml ampicillin as described (24), and EF-Ts from *E. coli* (using plasmid pCA24N*tsf* obtained from the ASKA collection (23)) was expressed in LB supplemented with 30 μg/ml of chloramphenicol. EF-Ts variants derived from *E. coli* were

grown at 37 °C in LB medium supplemented with 100 μg/ml ampicillin. The cells containing the respective plasmid were grown to the mid-log phase (A_{600} = 0.6) and induced with 1 mM isopropyl thio-β-galactoside. Following induction the temperature was reduced to 25 °C for 2 h and then to 16 °C overnight. The cells were harvested by centrifugation as described above.

Similar purification procedures were followed for EF-Tu from *E. coli* and *P. aeruginosa*, as well as EF-Ts variants from *P. aeruginosa* and EF-Ts from *E. coli* (23). The cell pellets were resuspended in 7 ml of buffer A (50 mM Tris-Cl pH 8.0 (4 °C), 60 mM NH_4Cl, 7 mM $MgCl_2$, 300 mM KCl, 7 mM β-mercaptoethanol, 1 mM PMSF, 10 mM imidazole, 15% glycerol, and 50 μM GDP) per gram of cells and lysed with 1 mg/ml lysozyme. Cell debris was removed through centrifugation at 3000 × *g* for 30 min followed by 30,000 × *g* for 45 min using a JA-16 rotor (Beckman). The respective protein was purified from the cleared lysate (S30 extract) using affinity chromatography (7 ml of Ni^{2+}-Sepharose resin (GE Healthcare) equilibrated with buffer A). The resin was washed three times with 50 ml of buffer A and four times with 50 ml of buffer B (buffer A with 20 mM imidazole). The protein was eluted in 10 washes of 7 ml of buffer C (buffer A with 250 mM imidazole). The obtained His_6-tagged protein was then concentrated via ultrafiltration (Vivaspin 20, 30,000 MWCO for EF-Tu and Vivaspin 20, 10,000 MWCO for EF-Ts (Sartorius)) and further purified by size exclusion chromatography (XK26/100 column; Superdex 75 prep grade (GE Healthcare)) equilibrated in buffer E (Buffer A without GDP). Fractions were analyzed by SDS-PAGE, and those containing protein that was >90% pure were pooled, concentrated via ultrafiltration (see above), and stored at −80 °C. The final protein concentration was determined spectrophotometrically at 280 nm using a molar extinction coefficient of 32,900 M^{-1} cm^{-1} for EF-Tu (calculated using ProtParam (25)) and confirmed using Bradford Protein Assay (Bio-Rad).

EF-Ts variants from *E. coli* were purified using the following method. The cell pellets were resuspended in 7 ml of buffer E (25 mM Tris-Cl, pH 7.5 (4 °C), 50 mM NH_4Cl, 10 mM $MgCl_2$, 0.1% PMSF, and 50 μM GDP) per gram of cells and lysed with 1 mg/ml of lysozyme. Cell debris was removed via centrifugation as above to obtain a cleared lysate (S30 extract). The respective protein was purified from the cleared lysate using affinity chromatography (5 ml of chitin beads (New England BioLabs)) equilibrated with buffer E. The resin was washed three times with 50 ml of buffer E and five times with 50 ml of buffer F (20 mM Tris-Cl, pH 8.0 (4 °C), 50 mM NH_4Cl, 0.1 mM EDTA and 50 μM GDP). Approximately 20 ml of buffer G (20 mM Tris-Cl, pH 8.0 (4 °C), 50 mM NH_4Cl, 0.1 mM EDTA, 60 mM DTT, and 400 mM KCl) was added to induce release of EF-Ts caused by the cleavage of the intein fusion followed by incubation for ~30 h at room temperature. The EF-Ts protein was eluted with 8 washes of 4.5 ml of buffer H (20 mM Tris-Cl, pH 8.0 (4 °C), 50 mM NH_4Cl, 0.1 mM EDTA, 400 mM KCl, and 50 μM GDP). Elutions containing EF-Ts were pooled and concentrated via ultrafiltration (Vivaspin 20, 10,000 MWCO (Sartorius)) and subsequently subjected to size exclusion chromatography (XK26/100 column; Superdex 75 prep grade (GE Healthcare)) equilibrated in buffer A. The fractions were analyzed by SDS-PAGE, and those containing protein with a purity of >90% were pooled, concentrated via ultrafiltration (see above), and stored at −80 °C for further use. The final EF-Ts protein concentration was determined using Bradford protein assay (Bio-Rad).

Preparation of EF-Tu·mant-GDP and EF-Tu·mant-GTP—EF-Tu·GDP was incubated with a 10-fold molar excess of mant-GDP or mant-GTP in buffer A for 30 min at 37 °C. When mant-GTP was used, the incubations were carried out in the presence of 3 mM phosphoenolpyruvate and 0.1 mg/ml pyruvate kinase (Roche Diagnostics) to convert any nucleotide di-phosphate present into the nucleotide triphosphate form (26).

Preparation of Nucleotide-free EF-Tu and EF-Tu·EF-Ts—To promote the dissociation of GDP, which is tightly bound to EF-Tu and co-elutes with the factor during purification, EF-Tu·GDP was incubated in buffer I (25 mM Tris-Cl, pH 7.5 (20 °C), 50 mM NH_4Cl, 10 mM EDTA) for 30 min at 37 °C. GDP and EF-Tu were separated using size exclusion chromatography (Acorn 10/300 GL column; Superdex 75 (GE Healthcare)) equilibrated in buffer J (25 mM Tris-Cl pH 7.5 (4 °C), 50 mM NH_4Cl). To prepare the respective EF-Tu·EF-Ts complexes, EF-Tu·GDP was incubated with equimolar amounts of EF-Ts in buffer I and subsequently treated as described above.

Rapid Kinetics—Fluorescence stopped flow measurements were performed using a stopped flow apparatus (KinTek SF-2004), as described in Ref. 27. Tryptophan fluorescence was excited at 280 nm and measured after passing through LG-305-F cut-off filters (NewPort). Mant-nucleotides were excited via FRET from the single tryptophan (λ_{ex} = 280 nm) present in EF-Tu and measured after passing through LG-400-F cut-off filters (NewPort).

The apparent rate for the bimolecular association of mant-nucleotides to nucleotide-free EF-Tu was determined by rapidly mixing 25 μl of nucleotide free *E. coli* EF-Tu (0.3 μM after mixing) or 25 μl of nucleotide free *P. aeruginosa* EF-Tu (0.5 μM after mixing) with 25 μl of varying concentrations of mant-nucleotides (ranging from 1 to 10 μM after mixing) to ensure pseudo-first order conditions. The experiments were carried out at 20 °C in buffer A. Fluorescence time courses were evaluated by fitting with a single exponential equation (Equation 1),

$$F(t) = F_\infty + A \times \exp(-k \times t) \qquad \text{(Eq. 1)}$$

where $F(t)$ is the fluorescence at time t, F_∞ is the fluorescence signal at equilibrium, and k is the apparent rate constant of association (k_{app}) measured independently for each guanine nucleotide concentration. The apparent rate constants were then plotted as a function of nucleotide concentration.

The apparent rate for the bimolecular association of nucleotides to nucleotide free EF-Tu·EF-Ts was determined by rapidly mixing 25 μl of nucleotide free EF-Tu·EF-Ts (final concentration, 0.5 μM) with 25 μl of varying concentrations of guanine nucleotides (ranging from 2.5 to 1000 μM after mixing) at 20 °C in buffer A. Fluorescence time courses were fitted with Equation 1, and the values obtained were plotted as a function of increasing guanine nucleotide concentration.

Dissociation rate constants were determined by rapidly mixing 25 μl of EF-Tu·mant-GTP/mant-GDP (final concentration, 0.3 μM) with 25 μl of GTP/GDP (final concentration, 30 μM) at

20 °C in buffer A. The observed fluorescence time courses were fitted with Equation 1, and the resulting k provided the dissociation rate constant (k_{-1} and k_{-5} for GDP and GTP, respectively). Using similar conditions, the dissociation of mant-GTP/mant-GDP from 25 μl of EF-Tu·mant-GTP/GDP (0.3 μM after mixing) was stimulated with 25 μl of varying concentrations of EF-Ts (1–20 μM after mixing) at 20 °C in buffer A. The observed fluorescence time courses were fitted with Equation 1, providing the rate of nucleotide dissociation in the presence of different concentrations of EF-Ts, yielding k_{-7} and k_{-4} at saturation.

To determine the association rate constants (k_2) for the EF-Tu·EF-Ts interaction, increasing concentrations of EF-Ts (final concentration, 1–5 μM) were mixed with nucleotide-free EF-Tu (final concentration, 1 μM), and the resulting decrease in tryptophan fluorescence was observed as a function of time. The resulting concentration dependence of the observed association rates yielded the respective k_2.

Equilibrium binding constants (K_d) were calculated from the respective rate constants (k and k_-). The corresponding error (σ_{Kd}) was calculated using Equation 2.

$$\sigma_{Kd} = K_d \times \sqrt{((\sigma_{k_-}/k_-)^2 + (\sigma_k/k)^2)} \qquad \text{(Eq. 2)}$$

The calculations were performed using TableCurve (Jandel Scientific) and Prism (GraphPad Software).

Sequence Alignment—Protein primary sequences for EF-Ts and EF-Tu were obtained from the ExPASy website (Swiss-Prot database) (28), and the generated multiple sequence alignments (CLUSTALW (29)) were analyzed using GeneDoc (30).

Construction of EF-Tu·EF-Ts Models in Silico—A model of the *E. coli* EF-Tu·EF-Ts complex was constructed using the x-ray structure of this complex solved by Leberman and coworkers (16). This model lacked atomic coordinates for the N terminus (amino acids 1–8) and switch I regions of EF-Tu, which were presumably disordered in the crystal. A model for the N terminus of EF-Tu was obtained from the crystal structure of EF-Tu·GDPNP (7). The only conformation of switch I of EF-Tu available in the Protein Data Bank that is compatible with the presence of the C-terminal module of EF-Ts is found in a model of EF-Tu bound to the ribosome (31). The C terminus of EF-Ts(Chimera) was modeled by extending the *E. coli* EF-Ts model using Swiss-Pdb Viewer software (32). This model was solvated in a box of water molecules that extended 10 Å from the protein in each direction, and the aqueous system was minimized by relaxing the coordinates of protein, water, protein, and water in sequential energy minimization calculations for 10,000 steps each. A final all-atom minimization was performed until no change in total energy was measured over 1000 steps. To alleviate close contacts with the switch I region and generate a disordered conformation, the switch I and the N terminus were subjected to simulated annealing. During simulated annealing only the water molecules, the N terminus and switch I region of EF-Tu, as well as the C-terminal extension of EF-Ts(Chimera) (when present), were allowed to move. The melting phase involved heating the system from 100 to 1000 K by increasing the temperature 100 K every 5 ps. The system was maintained at 1000 K for 150 or 300 ps prior to cooling to 300 K by decreasing the temperature 10 K every 5 ps. Each cooling phase was performed 10 times with different random velocities to yield a total of 20 different cooling trajectories. After reaching 300 K, each trajectory was extended for an additional 150 ps at 300 K. Simulated annealing was performed with constant volume to maintain close proximity of water molecules and the protein elements. Following simulated annealing, the protein complex was solvated in a new box of water molecules, and the aqueous system was again minimized as before (see above). The electrostatic charge of the model was then neutralized by addition of 24 Na^+ ions using the autoionize module in VMD (33).

Each model was then equilibrated in two independent simulations: at 300 and 350 K for 150 ps at 1 atm pressure using an NPT ensemble wherein the number of atoms, pressure, and temperature were kept constant. During equilibration the temperature was maintained using Langevin dynamics, and pressure was controlled by a Nosé-Hoover Langevin piston. At the start of each production phase simulation, the coordinates from the 350 K equilibration were cooled to 300 K by supplying the atomic velocities from the final step in the 300 K equilibration. Production phase simulations were carried out for 20 ns on each EF-Tu·EF-Ts model in an NPT ensemble; temperatures were maintained at 300 K by rescaling atomic velocities every 100 steps, and the Nosé-Hoover Langevin piston was used to maintain 1 atm pressure. All molecular dynamics simulations were carried out using the NAMD (34) software with a conservative step size of 0.5 fs/step and the CHARMM27 forcefield (35, 36).

Analysis of Molecular Dynamics Simulations—Snapshots of each MD simulation were saved every 2 ps, and trajectories were fitted by the software Carma (37) to remove water molecules, as well as any rotations of the protein complex or translation of the center of mass. All metrics in the simulation were measured in VMD (33) using scripts written in-house (15, 17). Further processing of MD data and subsequent plotting were performed using the software R (38). Quantitative analysis of hydrogen bonds was performed as previously described (15, 17).

Author Contributions—H.-J. W., E. D., and E. M. wrote the manuscript, E. D. performed all experiments, and E. M. all performed molecular dynamic simulations. H.-J. W. conceived and designed the study.

Acknowledgments—We thank Ute Kothe for critical reading of the manuscript, as well as Fan Mo, Adam Smith, and Emily Wilton for technical assistance.

References

1. Arike, L., Valgepea, K., Peil, L., Nahku, R., Adamberg, K., and Vilu, R. (2012) Comparison and applications of label-free absolute proteome quantification methods on *Escherichia coli*. *J. Proteomics* **75,** 5437–5448
2. Miller, D. L., and Weissbach, H. (1977) Factors involved in the transfer of aminoacyl transfer RNA to the ribosome. In *Molecular Mechanisms of Protein Biosynthesis* (Weissbach, H., and Petska, S., eds) pp. 323–373, University of Michigan Press, Ann Arbor, MI
3. Pingoud, A., Gast, F. U., Block, W., and Peters, F. (1983) The elongation factor-Tu from *Escherichia coli*, aminoacyl-transfer RNA, and guanosine tetraphosphate form a ternary complex which is bound by programmed ribosomes. *J. Biol. Chem.* **258,** 14200–14205

4. Rodnina, M. V., Gromadski, K. B., Kothe, U., and Wieden, H. J. (2005) Recognition and selection of tRNA in translation. *FEBS Lett.* **579,** 938–942
5. Pape, T., Wintermeyer, W., and Rodnina, M. V. (1998) Complete kinetic mechanism of elongation factor Tu-dependent binding of aminoacyl-tRNA to the A site of the *E. coli* ribosome. *EMBO J.* **17,** 7490–7497
6. Kothe, U., and Rodnina, M. V. (2006) Delayed release of inorganic phosphate from elongation factor Tu following GTP hydrolysis on the ribosome. *Biochemistry* **45,** 12767–12774
7. Kjeldgaard, M., and Nyborg, J. (1992) Refined structure of elongation factor EF-Tu from *Escherichia coli*. *J. Mol. Biol.* **223,** 721–742
8. Song, H., Parsons, M. R., Rowsell, S., Leonard, G., and Phillips, S. E. (1999) Crystal structure of intact elongation factor EF-Tu from *Escherichia coli* in GDP conformation at 2.05 Å resolution. *J. Mol. Biol.* **285,** 1245–1256
9. Gromadski, K. B., Wieden, H. J., and Rodnina, M. V. (2002) Kinetic mechanism of elongation factor Ts-catalyzed nucleotide exchange in elongation factor Tu. *Biochemistry* **41,** 162–169
10. Chau, V., Romero, G., and Biltonen, R. L. (1981) Kinetic studies on the interactions of *Escherichia coli* K12 elongation factor Tu with GDP and elongation factor Ts. *J. Biol. Chem.* **256,** 5591–5596
11. Young, R., and Bremer, H. (1976) Polypeptide-chain-elongation rate in *Escherichia coli* B/r as a function of growth-rate. *Biochem. J.* **160,** 185–194
12. Andersen, G. R., Pedersen, L., Valente, L., Chatterjee, I., Kinzy, T. G., Kjeldgaard, M., and Nyborg, J. (2000) Structural basis for nucleotide exchange and competition with tRNA in the yeast elongation factor complex eEF1A:eEF1Bα. *Mol. Cell* **6,** 1261–1266
13. Dahl, L. D., Wieden, H. J., Rodnina, M. V., and Knudsen, C. R. (2006) The importance of P-loop and domain movements in EF-Tu for guanine nucleotide exchange. *J. Biol. Chem.* **281,** 21139–21146
14. Wieden, H. J., Gromadski, K., Rodnin, D., and Rodnina, M. V. (2002) Mechanism of elongation factor (EF)-Ts-catalyzed nucleotide exchange in EF-Tu: contribution of contacts at the guanine base. *J. Biol. Chem.* **277,** 6032–6036
15. Wieden, H. J., Mercier, E., Gray, J., Steed, B., and Yawney, D. (2010) A combined molecular dynamics and rapid kinetics approach to identify conserved three-dimensional communication networks in elongation factor Tu. *Biophys. J.* **99,** 3735–3743
16. Kawashima, T., Berthet-Colominas, C., Wulff, M., Cusack, S., and Leberman, R. (1996) The structure of the *Escherichia coli* EF-Tu·EF-Ts complex at 2.5 Å resolution. *Nature* **379,** 511–518
17. Mercier, E., Girodat, D., and Wieden, H. J. (2015) A conserved P-loop anchor limits the structural dynamics that mediate nucleotide dissociation in EF-Tu. *Sci. Rep.* **5,** 7677
18. Rosler, K. S., Mercier, E., Andrews, I. C., and Wieden, H. J. (2015) Histidine 114 is critical for ATP hydrolysis by the universally conserved ATPase YchF. *J. Biol. Chem.* **290,** 18650–18661
19. Gromadski, K. B., Schümmer, T., Strømgaard, A., Knudsen, C. R., Kinzy, T. G., and Rodnina, M. V. (2007) Kinetics of the interactions between yeast elongation factors 1A and 1Bα, guanine nucleotides, and aminoacyl-tRNA. *J. Biol. Chem.* **282,** 35629–35637
20. Schümmer, T., Gromadski, K. B., and Rodnina, M. V. (2007) Mechanism of EF-Ts-catalyzed guanine nucleotide exchange in EF-Tu: contribution of interactions mediated by helix B of EF-Tu. *Biochemistry* **46,** 4977–4984
21. Zhang, Y., Yu, N. J., and Spremulli, L. L. (1998) Mutational analysis of the roles of residues in *Escherichia coli* elongation factor Ts in the interaction with elongation factor Tu. *J. Biol. Chem.* **273,** 4556–4562
22. Boon, K., Vijgenboom, E., Madsen, L. V., Talens, A., Kraal, B., and Bosch, L. (1992) Isolation and functional-analysis of histidine-tagged elongation-factor Tu. *Eur. J. Biochem.* **210,** 177–183
23. Kitagawa, M., Ara, T., Arifuzzaman, M., Ioka-Nakamichi, T., Inamoto, E., Toyonaga, H., and Mori, H. (2005) Complete set of ORF clones of *Escherichia coli* ASKA library (A complete set of *E. coli* K-12 ORF archive): unique resources for biological research. *DNA Res.* **12,** 291–299
24. De Laurentiis, E. I., Mo, F., and Wieden, H. J. (2011) Construction of a fully active Cys-less elongation factor Tu: functional role of conserved cysteine 81. *Biochim. Biophys. Acta* **1814,** 684–692
25. Wilkins, M. R., Gasteiger, E., Bairoch, A., Sanchez, J.-C., Williams, K. L., Appel, R. D., and Hochstrasser, D. F. (1999) Protein identification and analysis tools in the ExPASy Server. *Methods Mol. Biol.* **112,** 531–552
26. Scolnick, E., Tompkins, R., Caskey, T., and Nirenberg, M. (1968) Release factors differing in specificity for terminator codons. *Proc. Natl. Acad. Sci. U.S.A.* **61,** 768–774
27. Shields, M. J., Fischer, J. J., and Wieden, H. J. (2009) Toward understanding the function of the universally conserved GTPase HflX from *Escherichia coli*: a kinetic approach. *Biochemistry* **48,** 10793–10802
28. Gasteiger, E., Gattiker, A., Hoogland, C., Ivanyi, I., Appel, R. D., and Bairoch, A. (2003) ExPASy: the proteomics server for in-depth protein knowledge and analysis. *Nucleic Acids Res.* **31,** 3784–3788
29. Larkin, M. A., Blackshields, G., Brown, N. P., Chenna, R., McGettigan, P. A., McWilliam, H., Valentin, F., Wallace, I. M., Wilm, A., Lopez, R., Thompson, J. D., Gibson, T. J., and Higgins, D. G. (2007) Clustal W and Clustal X version 2.0. *Bioinformatics* **23,** 2947–2948
30. Nicholas, K. B., Nicholas, H. B. J., and Deerfield, D. W. (1997) GeneDoc: Analysis and visualization of genetic variation. *Embnew. News* **4**
31. Villa, E., Sengupta, J., Trabuco, L. G., LeBarron, J., Baxter, W. T., Shaikh, T. R., Grassucci, R. A., Nissen, P., Ehrenberg, M., Schulten, K., and Frank, J. (2009) Ribosome-induced changes in elongation factor Tu conformation control GTP hydrolysis. *Proc. Natl. Acad. Sci. U.S.A.* **106,** 1063–1068
32. Guex, N., and Peitsch, M. C. (1997) SWISS-MODEL and the Swiss-Pdb Viewer: an environment for comparative protein modeling. *Electrophoresis* **18,** 2714–2723
33. Humphrey, W., Dalke, A., and Schulten, K. (1996) VMD: visual molecular dynamics. *J. Mol. Graph.* **14,** 33–38
34. Phillips, J. C., Braun, R., Wang, W., Gumbart, J., Tajkhorshid, E., Villa, E., Chipot, C., Skeel, R. D., Kalé, L., and Schulten, K. (2005) Scalable molecular dynamics with NAMD. *J. Comput. Chem.* **26,** 1781–1802
35. Foloppe, N., and Mackerell, A. D. (2000) All-atom emperical force field for nucleic acids: I. parameter optimization based on small molecule and condensed phase macromolecular target data. *J. Comput. Chem.* **21,** 86–104
36. MacKerell, A. D., Bashford, D., Bellott, M., Dunbrack, R. L., Evanseck, J. D., Field, M. J., Fischer, S., Gao, J., Guo, H., Ha, S., Joseph-McCarthy, D., Kuchnir, L., Kuczera, K., Lau, F. T., Mattos, C., *et al.* (1998) All-atom emperical potential for molecular modeling and dynamics studies of proteins. *J. Phys. Chem. B* **102,** 3586–3616
37. Glykos, N. M. (2006) Carma: A molecular dynamics analysis program. *J. Comput. Chem.* **27,** 1765–1768
38. RCoreTeam (2013) R: A language and environment for statistical computing. R Foundation for Statistical Computing, Vienna, Austria

The C-terminal Helix of *Pseudomonas aeruginosa* Elongation Factor Ts Tunes EF-Tu Dynamics to Modulate Nucleotide Exchange

Evelina Ines De Laurentiis, Evan Mercier and Hans-Joachim Wieden

J. Biol. Chem. 2016, 291:23136-23148.
doi: 10.1074/jbc.M116.740381 originally published online September 13, 2016
